Brown, Cameron J. and Adelakun, Juliet A. and Ni, Xiong wei (2015) Characterization and modelling of antisolvent crystallization of salicylic acid in a continuous oscillatory baffled crystallizer. Chemical Engineering and Processing: Process Intensification, 97. pp. 180-186. ISSN 0255-2701 , http://dx.doi.org/10.1016/j.cep.2015.04.012

Chemical Engineering and Processing 97 (2015) 180–186

Contents lists available at ScienceDirect

Chemical Engineering and Processing: Process Intensification

journal homepage: www.elsevier.com/locate/cep

Characterization and modelling of antisolvent crystallization of salicylic acid in a continuous oscillatory baffled crystallizer

Cameron J. Brown *, Juliet A. Adelakun, Xiong-wei Ni

EPSRC Centre for Innovative Manufacturing in Continuous Manufacturing and Crystallization, Heriot-Watt University, Edinburgh EH14 4AS, UK

ARTICLE INFO

Article history:
Received 28 February 2014
Received in revised form 30 March 2015
Accepted 27 April 2015
Available online 2 May 2015

Keywords:
Antisolvent
Continuous
Crystallization
Oscillatory baffled crystallizer
Population balance
Kinetics

ABSTRACT

Using antisolvent crystallisation of salicylic acid as the model process, we report our experimental investigation into the temporal and spatial steady states of solution concentration and mean crystal size in a continuous oscillatory baffled crystallizer. The evolutions of the two parameters over time and distance along the crystallizer are measured for a variety of operating conditions. The results show that the attainment of long term temporal and spatial stabilities (>100 residence times) for the solute concentrations are easily achieved, whereas the temporal steady states of the mean crystal size are more difficult to accomplish, even though the spatial steady states have been obtained. A simplified population balance model is applied to the experimental data for the determination of nucleation and growth kinetic parameters. From which both the solution concentration and the mean size were predicted and matched to experimental values reasonably well. In addition, we have identified and executed the conditions of long term steady states for extended operation of 6.25 h to produce close to 1 kg of crystal product with minimal variation in crystal size (±3.01 μm).

1. Introduction

For the bulk, fine chemicals, food and pharmaceutical industries, crystallization is a key separation and purification process. In the pharmaceutical industry alone, over 90% of all active pharmaceutical ingredients (API) would go through a crystallization step at some stage of their production cycles [1]. One of the more common crystallization processes is that of antisolvent crystallization. This involves the mixing of two miscible fluids: an API dissolved in a solvent and an antisolvent which reduces the solubility of API in the solvent, causing the API to crystallize out of the solution. One parameter of significance is the crystal size distribution as this affects the efficiency of downstream processes (e.g. filtration, washing, drying, etc.) and the properties of the crystals (e.g. storage characteristics, bioavailability, compactibility, tabletability, etc.). The size and shape of crystal size distribution is governed by a balance between the nucleation and crystal growth processes which are in themselves proportional to the level of supersaturation.

Continuous crystallizers can take many forms, but are broadly separated into two categories: mixed suspension mixed product removal (MSMPR) or plug flow (PF). MSMPR crystallizers tend to take the format of a cascade of stirred tank crystallizers (STC), whereas PF crystallizers follow a tubular configuration. Within the PF crystallizer category, numerous designs have been developed, such as a T-mixer used by Stahl et al. [2] for the reactive crystallization of benzoic acid, Gradl et al. [3] for the precipitation of barium sulphate nanoparticles and by Blandin et al. [4] for the precipitation of salicylic acid. Static mixers have also been studied for PF crystallization, for example, the Kenics mixer used by Rivera and Randolph [5] for the precipitation of PETN and more recently by Alvarez and Myerson [6] for the antisolvent crystallizations of ketoconazole, flufenamic acid and L-glutamic acid. Simon and Myserson [7] also carried out the antisolvent crystallization of butamben in the same Kenics setup used previously [6], but with the addition of copper-hydroxide tracer to monitor the plug flow dispersion. Finally, Lawton et al. [8] deployed a continuous oscillatory baffled crystallizer (COBC) to achieve PF for the cooling crystallization of a proprietary API.

One of the key challenges in the successful operation of a continuous crystallization is the monitoring and control of the system. Nagy et al. [9] carried out a detailed review of the use and current challenges for population balance modelling for crystallization systems. In conjunction, they also discuss the development of process analytical techniques (PAT) for crystallization monitoring. Finally, they discuss appropriate control strategies using a combination of PAT and population balance modelling. More

* Corresponding author at: Institute of Mechanical, Process and Energy Engineering, Heriot-Watt University, Edinburgh EH14 4AS, Scotland, UK. Tel.: +44 131 451 3590.
E-mail address: cameron.j.brown@hw.ac.uk (C.J. Brown).

http://dx.doi.org/10.1016/j.cep.2015.04.012

recently, Simon et al. review [10] provides a wide overview of the current state of PAT and its implementation.

Mixing plays an important role in any crystallization [11], even more so in antisolvent processes where uniformly distribution of the antisolvent throughout the system is essential. Therefore, it is desirable to have a mixing time less than the induction time of crystallization, which is easily achievable in confined impinging jet arrangements for a range of crystallization systems [12,13]. However, up scaling of these arrangements is complicated [14] and can be blocked easily if miss aligned.

A potential alternative could be the application of a COBC as it offers a rapid mixing time [15] but is readily scalable [16]. COBC has previously been shown to produce consistent crystal size and morphology; reduce crystallization time, space usage, utility and energy consumption [8]; have also demonstrated the ability to produce a single form of crystal when two forms are possible [17] and product crystals of higher quality (in terms of size distribution and surface characteristics) when compared to that of stirred systems [18].

The aims of this work are to study, for the first time, an antisolvent crystallization of an API substitute in a COBC to generate seed crystals; in particular, to examine the steady states of solute concentration and mean crystal size with regards to both the operating time (temporal) and the distance along the crystallizer (spatial). In addition, a simplified population balance model is applied to the experimental data for the determination of nucleation and growth kinetic parameters, which is again a first for a COBC system.

2. Experimental

2.1. Materials

Salicylic acid (*ortho*-hydroxybenzoic acid) is widely known for its analgesic, fever relief and anti-inflammatory properties and is more commonly found in its prodrug form of aspirin (acetylsalicylic acid). It has a very low solubility in water but is highly soluble in a wide range of organic solvents (methanol, ethanol, 2-propanol and THF). Unlike its isomers (*p*- and *m*-hydroxybenzoic acid), no polymorphs or solvates of salicylic acid have been encountered [19].

Salicylic acid (99.5%, Acros Organics) and 2-propanol (99.5%, Acros Organics) were both purchased from Fisher Scientific. Distilled water was obtained from a Fisons FI-Streem water still.

2.2. Experimental apparatus

A continuous oscillatory baffled crystallizer based on previous designs [8] was fabricated and modified for the use in antisolvent crystallizations. A schematic diagram of the experimental setup is shown in Fig. 1. The system consisted of two straight sections converging into a third straight section, via a *y*-piece, each section was a jacketed glass tube Ø15 mm × 700 mm with PVDF (polyvinylidene fluoride) baffle inserts fitted throughout. Solvent and antisolvent were held in two 20 l jacketed stirred tanks and connected to the crystallizer via peristaltic pumps (Watson Marlow) through 3.2 mm santoprene tubing (1.6 mm wall thickness). Oscillation was supplied by a PTFE (polytetrafluoroethylene) bellows and linear actuator (Dunkermotoren) configuration to one of the straight inlet sections. Temperature was controlled by circulating water through the section jackets via a recirculation chiller (Neslab). Additional sampling collars were fitted between the outlet of the *y*-piece (55 mm from the mixing point where the two streams meet, denoted as C_1 and $L_{32,1}$ in Fig. 1) and at the end of the third straight outlet (785 mm from the mixing point, denoted as C_2 and $L_{32,2}$ in Fig. 1) to allow for the monitoring of the crystallization process.

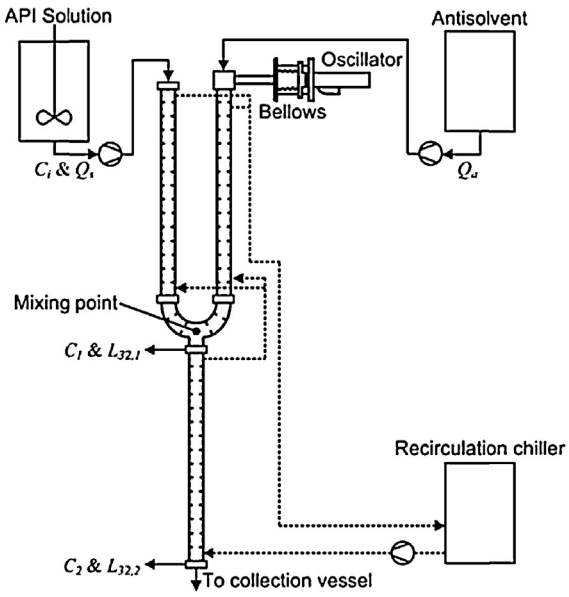

Fig. 1. Schematic of modified COBC for antisolvent crystallization.

Sample solute concentration was measured by FTIR spectroscopy with a wavenumber range of 600–2000 cm^{-1}. A FTIR spectrophotometer (Shimadzu IRPrestige-21) was equipped with an ATR accessory (Specac ATR with high throughput diamond). Concentration of salicylic acid was measured by following the peak height between 1631 and 1647 cm^{-1}.

The crystal size distribution of the solid product of the samples was carried out by laser diffraction (Malvern Mastersizer S) with a measurement range of 0.1–300 μm. Solid samples were added via a wet dispersion unit and agitated at 800 rpm where chilled distilled water was the dispersing fluid.

2.3. Procedure

All experiments were performed isothermally at 25 °C. A saturated 54 vol% water/2-propanol solution of salicylic acid (0.096 g/ml) and water (antisolvent) were added to the crystallizer (previously filled with 2-propanol) using the peristaltic pumps. The flow rate of the saturated solution was maintained at 40 ml/min throughout all experiments and the initial supersaturation was studied and verified by running experiments with 40, 60 and 80 ml/min of antisolvent. Additionally, the oscillation frequency was maintained at 5 Hz across all experiments, but the effect of oscillation conditions was investigated by undertaking experiments with equal flow rates of both solution and antisolvent at amplitudes of 5, 10 and 20 mm, respectively. A summary of all experimental conditions is shown in Table 1.

Unlike dynamic batch crystallization processes, continuous processes eventually reach a steady state operation, in terms of both temporal and spatial dimensions when dealing with tubular configurations. A steady state operation in this work was defined as the longest period of operation for which the standard deviation of parameters of interest was less than 10% of their mean values. A commonly quoted value for the time period to achieve steady state is between 4 and 10 residence times from start-up [6,20]. To ensure that a steady state operation was achieved, the total duration of the experiments ranged from 50 to 180 times the residence time in this work.

Table 1
Experimental conditions.

Exp.	Solution flow rate ml/min	Antisolvent flow rate ml/min	Mean residence time min	Oscillation amplitude mm	Initial supersaturation ratio C/C_{sat}
A	40	40	1.50	5	5.56
B	40	40	1.50	10	5.56
C	40	40	1.50	20	5.56
D	40	60	1.25	20	8.16
E	40	80	1.00	20	11.71

Samples were withdrawn from both sample points of the crystallizer at 15 min intervals and filtered with a 0.45 μm syringe filter (Millipore) to determine the solute concentration via FTIR spectroscopy as described previously. Samples of the slurry from each sample point were also taken and filtered with a 1.2 μm filter (Whatman GF/C) on a Buchner funnel under vacuum and the solid phase dried overnight at 60 °C. Crystal size distribution of the solid phase was then characterized by dispersing sufficient material in 130 ml of dispersing fluid to achieve a 20% obscuration.

3. Population balance model

The population balance equation for a plug flow crystallizer at steady state can be written as [6,21]:

$$u_x\frac{\delta n}{\delta x}+G\frac{\delta n}{\delta L}=0 \tag{1}$$

where n is the number density, x the distance along the crystallizer, G the crystal growth rate and L the crystal size. Additionally, u_x is the average net velocity of the fluid and is computed by summating the total volumetric flow rates of solution and antisolvent and dividing by the cross-sectional area of the crystallizer. Assuming no seeding or solids present at the mixing point, the boundary conditions for Eq. (1) are defined as:

$$n(0,x)=\frac{B_0}{G} \tag{2}$$

$$n(L,0)=0 \tag{3}$$

In addition to the population balance of Eq. (1), consideration of the energy and mass balances of the system must also be undertaken. Since the crystallization was maintained at isothermal conditions, i.e. the heat of crystallization is negated, the energy balance does not need to be calculated and the mass balance of the solute can be expressed by:

$$u_x\frac{dC}{dx}=-3\rho_c k_v G\int_0^\infty L^2 n dL \tag{4}$$

where C is the concentration of solute in the liquid phase, ρ_c the solid crystal density and k_v the crystal volume shape factor. Supplementary equations further consist of the nucleation rate, B_0, and the growth rate, G, in the following expressions:

$$B_0=k_b\Delta C^b \tag{5}$$

$$G=k_g\Delta C^g \tag{6}$$

Together with the percentage ratio of antisolvent, W, the supersaturation, ΔC, and the solubility curve, C_{sat}:

$$W=\frac{100Q_a}{Q_a+Q_b} \tag{7}$$

$$\Delta C=C-C_{sat} \tag{8}$$

$$C_{sat}=A_{fit}\exp(-B_{fit}W) \tag{9}$$

where k_b,b, k_g and g are the kinetic parameters, Q_a and Q_s are the antisolvent and solvent volumetric flow rate, respectively, ΔC the supersaturation, C_{sat} the solubility concentration and A_{fit} and B_{fit} are fitted parameters for the solubility curve [22].Solutions of the population equation can be obtained by numerous methods. For this application, the method of moments (MOM) was chosen for its cheap computational evaluation, where a moment is defined as:

$$\mu_k=\int_0^\infty L^k n(L,x)dL \tag{10}$$

Applying a moment transformation to the original population balance equation for the first 4 moments, plus the mass balance equation yields the following system of differentials:

$$\begin{bmatrix}\frac{d\mu_0}{dx}\\ \frac{d\mu_1}{dx}\\ \frac{d\mu_2}{dx}\\ \frac{d\mu_3}{dx}\\ \frac{dC}{dx}\end{bmatrix}=\begin{bmatrix}\frac{B_0}{u_x}\\ \frac{G\mu_0}{u_x}+\frac{B_0L_0}{u_x}\\ \frac{2G\mu_1}{u_x}+\frac{B_0L_0^2}{u_x}\\ \frac{3G\mu_2}{u_x}+\frac{B_0L_0^3}{u_x}\\ \frac{-3p_c k_v G\mu_2}{u_x}\end{bmatrix} \tag{11}$$

The calculations of the 2nd and 3rd moments allow for the determination of the area mean size (L_{32}) of the crystal size distribution:

$$L_{32}=\frac{\mu_3}{\mu_2} \tag{12}$$

Solutions of the system of differentials in Eq. (11) were obtained by utilizing a Runge–Kutta numerical integration. Initial conditions for Eq. (11) were taken as: $\mu_i(0)=0$ ($i=0, 1 \ldots 3$) and $C(0)=C_i$. Estimation of the kinetic parameters was undertaken by employing a multiobjective genetic algorithm to minimise the sum of squares of the error, where the error was defined as the absolute relative error between the experimental measurements and the model predications. The values L_{32} and C were chosen as the two objectives for the algorithm. Numerical figures for all the parameters discussed are given in Table 2. Note that as this method of population balance modelling does not take into consideration of any hydrodynamic effects, only those experiments which altered the crystallization parameters, e.g. the antisolvent flow rate in Table 2, were modelled, i.e. exp. C–E in Table 1.

Table 2
Parameters for population balance modelling.

Parameter	Value	Unit
Initial solute concentration, C_i	0.096	g/ml
Crystal density, ρ_c	1.443	g/ml
Volume shape factor, k_v	4.08	
Solvent volumetric flow rate, Q_s	18	ml/min
Antisolvent volumetric flow rate, Q_a	62, 82, 102	ml/min
Inner diameter, d_i	0.015	m
Solubility parameter, A_{fit}	1.643	g/ml
Solubility parameter, B_{fit}	0.05431	
Nucleation rate constant, $\ln(k_b)$	30.50 ± 0.30	$\#/m^3\,s$
Nucleation order, b	1.03 ± 0.03	
Growth rate constant, $\ln(-k_g)$	1.49 ± 0.35	m/s
Growth order, g	1.16 ± 0.05	

4. Results and discussion

4.1. Effect of mixing intensity on experimental steady states

The solute concentrations and the mean crystal sizes were obtained at two sample locations during each experiment and can be used to analyse the degree of steady states of the two parameters. Fig. 2 shows the experimental profiles of the solute concentration, C_1 and C_2, and the mean crystal size, $L_{32,1}$ and $L_{32,2}$ (shown in Fig. 1) as a function of the number of residence times, τ, for exp. A and B.

For both experiments, it can be seen that the solute concentration (the top graphs in Fig. 2) reached its steady state values at both sampling locations at the first sampling time (15 min or 10 τ) (Exp. A: $C_1 = 0.0187 \pm 0.0007$ g/ml, $C_2 = 0.0187 \pm 0.0002$ g/ml and Exp. B: $C_1 = 0.0199 \pm 0.0003$ g/ml, $C_2 = 0.0198 \pm 0.0002$ g/ml). This is consistent with the frequently quoted figure of 4 – 10 residence times to achieve steady state [6]. Furthermore, this steady state period was then maintained until the end of the exp. A and B of 50 and 70τ, respectively. The data suggest that the temporal steady state of solute concentration has been achieved during the operation.

With regards to the mean crystal size (the bottom graphs in Fig. 2), the steady state was achieved at both sampling locations in exp. A at the first sampling time (10τ), e.g. $L_{32,1} = 35.14 \pm 3.17$ μm and $L_{32,2} = 32.60 \pm 1.39$ μm. However, a reduction in the mean size was seen at both sampling locations towards the end of operation ($\geq 40\tau$), although the reduction was relatively small, it does suggest that the steady state of mean crystal size has been lost. This was further confirmed by the blockage of the crystallizer soon after this. A similar trend is seen for exp. B where the steady state mean size was achieved ($L_{32,1} = 58.19 \pm 4.22$ μm and $L_{32,2} = 52.28 \pm 1.89$ μm) at both sampling locations during early operation (20 and 10τ for $L_{32,1}$ and $L_{32,2}$, respectively), a similar but larger reduction in mean size followed towards the end of the experiment and once again the steady state was lost by 60τ, with the crystallizer being blocked soon after.

Note that the only variable in the operating conditions between exp. A and B was an increase in the oscillation amplitude from 5 to 10 mm (Table 1), with a longer operational period of 70τ in exp. B than that of 50τ in exp. A. Blockage prevented further operation in both cases. In order to maintain solid suspension and prevent blockage from occurring, the oscillation amplitude was increased further to 20 mm in exp. C. Fig. 3 shows the profiles of C and L_{32} a function of τ for exp. C.

We can see that the steady state of solute concentration was reached at both sampling locations ($C_1 = 0.0205 \pm 0.0007$ g/ml and $C_2 = 0.0204 \pm 0.0007$ g/ml) by the first sampling time (10τ) and was maintained for the rest of the operation. A steady state for the mean size was quickly achieved at 20τ for both sampling locations ($L_{32,1} = 71.04 \pm 6.34$ μm and $L_{32,2} = 71.02 \pm 3.28$ μm), but was only maintained until 100 and 90τ for $L_{32,1}$ and $L_{32,2}$, respectively, at which point the mean size decreased out with the steady state boundaries. However, unlike the outcomes from the exp. A and B where blockage occurred soon after the steady state was lost, the operation in exp. C continued with no signs of blockage at all until the feed solution tank had been depleted (180 min). This confirms that the further increase in the oscillation amplitude has improved the overall mixing in the system and prevented blockage from happening, but the true steady state of the crystal mean size was still lost at the end of the operation.

In the first set of three experiments (A–C), the oscillation amplitude was successively increased in order to enhance the mixing intensity with the aim to ensure adequate suspension of the crystals and prevent blockage. Oscillatory baffled reactors are generally characterized in terms of their oscillatory Reynold number, Re_o [23], defined as:

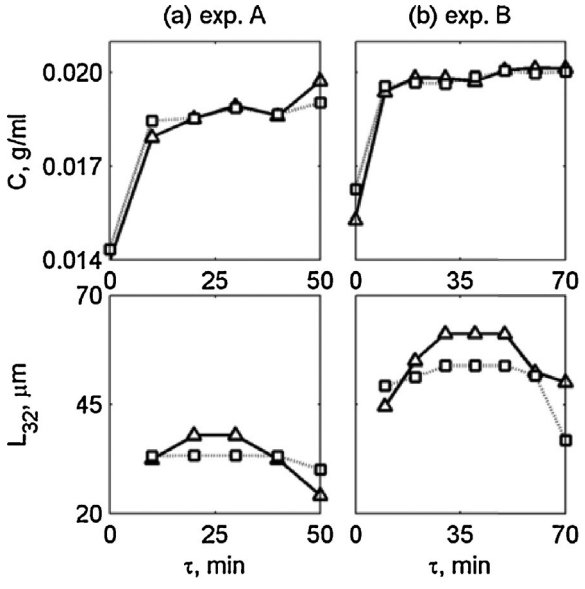

Fig. 2. Measurements of C_1 (△), C_2 (□), $L_{32,1}$ (△) and $L_{32,2}$ (□) for (a) exp. A and (b) exp. B as a function of τ. Note that the experimental duration for exp. A is 50 τ on the left and for exp. B is 70 τ on the right.

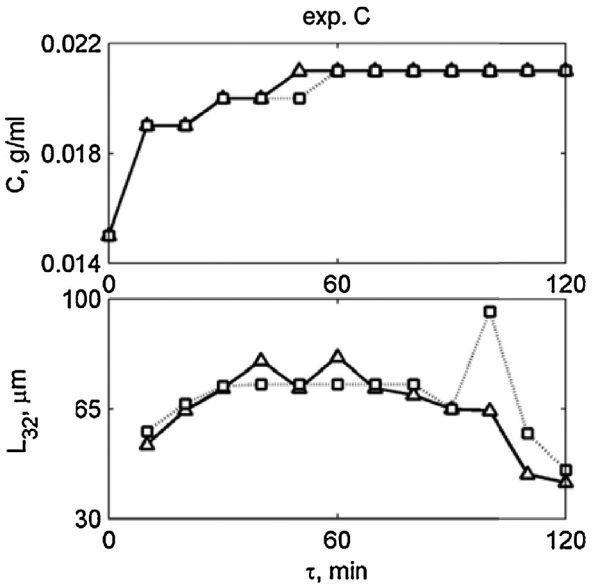

Fig. 3. Measurements of C_1 (Δ), C_2 (□), $L_{32,1}$ (Δ) and $L_{32,2}$ (□) for exp. C as a function of τ.

$$Re_o = \frac{2\pi f x_o D\rho}{\mu} \quad (13)$$

where, f is the oscillation frequency (Hz), x_o the oscillation centre to peak amplitude (m), D the column diameter (m), ρ the fluid density (kg/m^3) and μ the fluid viscosity (N s/m^2). Previous studies in batch oscillatory baffled crystallizers showed that an increase in Re_o, brought about by a change in either frequency or amplitude, led to a reduction in the mean crystal size [24,25] due to higher shear rates, in turn a higher dynamic nucleation rate with the production of more individual but smaller crystals. However, the results tabulated in Table 3 are contrary to this, showing that an increase in Re_o led to an increase in the mean size. The reasons for this were perhaps due to a combination of two factors, firstly larger crystals were difficult to maintain in suspension, secondly these crystals may have settled within the crystallizer. If so, effectively only the smaller crystals would have been suspended in the solution and sampled out at the sampling points. As a direct consequence of this, increasing the oscillatory Reynolds number would have brought about the suspension of larger crystals, in turn being sampled, resulting in a perceived increase in the mean crystal size. This is reflected in Fig. 2 were for both exp. A and B the mean size in sample position 1 is consistently higher than that in sample position 2 in the mid regions of the time axes. An occurance which was not observed for exp. C, as shown in Table 3.

4.2. Effect of supersaturation on experimental steady states

The effect of supersaturation on the steady states was investigated in exp. C–E by varying the flow rate of antisolvent as displayed in Table 1. Fig. 4 shows the variations of C_1, C_2, $L_{32,1}$ and $L_{32,2}$ as a function of the number of residence times, τ, for exp. D and E. Similar to all previous experiments, a steady state was achieved for the solute concentration (the top graphs in figure) by the first sampling time (12.5 and 15τ for exp. D and E, respectively) and was maintained for the remainder of operation. Both experiments experienced no blockage and were operated until the solution feed tank had been emptied, ~180 min.

The steady states of the mean crystal size (the bottom graphs in Fig. 4) are much more complicated and discussed in detail.

The mean crystal size in exp. D increased to a maximum by 60τ before decreasing. Applying the same definition of steady state would suggest that the steady state was maintained for $L_{32,1}$ at a value of 71.81 ± 6.57 μm between 50 and 137.5τ and for $L_{32,2}$ at 85.48 ± 8.08 μm between 25 and 137.5τ.

In comparison to exp. D, the mean crystal size did not exhibit the "bell" shape trend, but a continuing downward one with τ in exp. E. Using the steady state criteria suggests that $L_{32,1}$ was maintained at 54.39 ± 2.60 μm between 15 and 90τ and $L_{32,2}$ at 50.10 ± 4.34 μm between 15 and 150τ, however, the overall long term steady state for the mean crystal size was not achieved for both experiments. We postulate that this could potentially be due to the imbalance of flow rates at the mixer. As the flow rate of antisolvent stream was higher than that of the solution stream, the uptake of saturated solution could become sporadic leading to an inconsistent environment for crystal nucleation and growth. However, more detailed studies of the fluid dynamics of the mixer configuration would be required to fully justify this.

Table 3
Comparison of mean particle size versus oscillatory amplitude.

Exp.	Amplitude, x_o		Steady state mean size, μm	
	mm	Re_o	$L_{32,1}$	$L_{32,2}$
A	5	1141	35.14 ± 3.17	32.60 ± 1.39
B	10	2281	58.19 ± 4.22	52.28 ± 1.89
C	20	4562	71.04 ± 6.34	71.02 ± 3.28

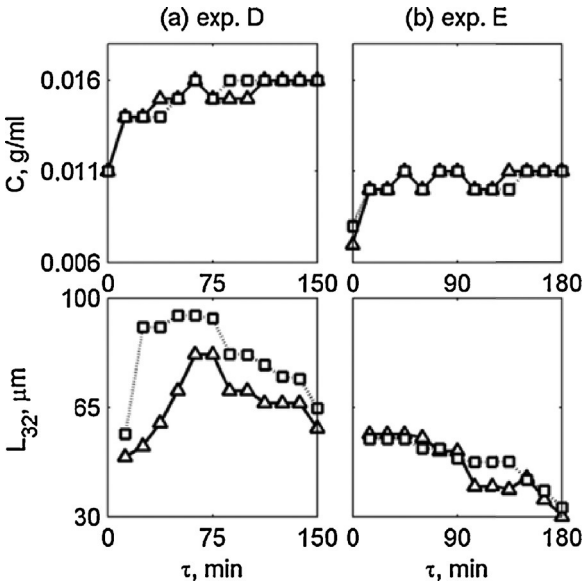

Fig. 4. Measurements of C_1 (Δ), C_2 (□), $L_{32,1}$ (Δ) and $L_{32,2}$ (□) for (a) exp. D and (b) exp. E as a function of τ. Note that the experimental duration for exp. D is 150 τ on the left and for exp. E is 180 τ on the right.

4.3. Experimental spatial steady states

Since the steady states in continuous operation involve both temporal, i.e. the variation as a function of time, and spatial dimensions (the variation with distance along the crystallizer), the spatial steady states can be assessed by comparing the values of the concentration and the mean crystal size between the two sampling locations (730 mm apart). A summary of such assessment for all experiments is given in Table 4. When comparing the values between sampling locations, i.e. C_1 vs. C_2 and $L_{32,1}$ vs. $L_{32,2}$, and considering the experimental errors, it can be seen that there is no statistic difference in either the solute concentration or the mean crystal size between the two locations, suggesting that a spatial steady state across the 730 mm section has been achieved. Furthermore this would infer that the solution has desupersaturated even before the first sampling location (55 mm from the mixing point of both the solution and the antisolvent).

4.4. Population balance modelling

The experimental data from exp. C–E (12 runs in total) were utilized for the kinetic parameter estimation using the population balance model described earlier. Using the estimated kinetic parameters (k_b, b, k_g and g) together with the physical data shown in Table 2, the population balance model minimised the error between the experimental data of both concentration and mean crystal size (Table 4) and the model predicted data. A graphical comparison of the experimental and the predicted data is shown in Fig. 5.

Looking at the predicted solute concentration profiles at the first measuring location (the top of Fig. 5), we see a rapid decrease

Table 4
Summary of all temporal steady state values.

Exp.	C_1 g/ml	C_2 g/ml	$L_{32,1}$ μm	$L_{32,2}$ μm
A	0.0187 ± 0.0007	0.0187 ± 0.0002	35.14 ± 3.17	32.60 ± 1.39
B	0.0199 ± 0.0003	0.0198 ± 0.0002	58.19 ± 4.22	52.28 ± 1.89
C	0.0205 ± 0.0007	0.0204 ± 0.0007	71.04 ± 6.34	71.02 ± 3.28
D	0.0151 ± 0.0007	0.0152 ± 0.0008	71.81 ± 6.57	85.48 ± 8.08
E	0.0106 ± 0.0004	0.0105 ± 0.0003	54.39 ± 2.60	50.10 ± 4.34

in the solute concentration from the mixing point (0 m) onwards, shortly after which the concentration is constant and remains so at the second measuring location (the top right of Fig. 5), leading to a complete desupersaturation of the solution. For all three flow rates of antisolvent modelled, the solute concentration has reached its steady state value by a distance of 16 mm from the mixing point of the solution and the antisolvent, this is consistent with the experimental data, supporting our earlier statement that the crystallization solution was desupersaturated at 55 mm from the point of mixing.

A similar rapid change is also seen in the mean crystal size which indicates that its steady state value was met at 24 mm from the point of mixing for each antisolvent flow rate (the bottom left of Fig. 5). However some variations in the experimental mean size took place between the first and second measuring locations, the predicted mean sizes only match the experimental measurements of 40 and 80 ml/min, within the experimental error, for both sampling locations. These conditions correspond to exp. C and E where the smallest variations in the steady state along the third straight section were found (Table 4). For the other runs, the true steady state in the mean crystal size has not been maintained.

4.5. Extended operation

As the operating conditions of exp. C showed the greatest potential for extended operation at steady states, exp. C was repeated for an overall operating time of 6.25 h (compared to 3 h in the initial experiment). In addition to this the plain glass tubes with PVDF baffle inserts were replaced with tubes with integrated glass baffles. The solute concentration and mean crystal size measurements for this extended run at the second sampling location are shown in Fig. 6.

We see that the concentration approached a steady state value of 0.0198 ± 0.0003 g/ml by 33τ and was remained for the duration of operation. The steady state of the mean crystal size of 44.63 ± 3.01 μm was also maintained for the entire duration from 17 to 250τ. This confirms our assessment. Of a particular note is the difference in the mean sizes between the initial exp. C (71.02 ± 3.28 μm) and the extended experiment here (44.63 ± 3.01 μm). The reason for this could be due to the construction as well as the change of baffle materials from PVDF inserts to integrated glass. The effect of this could be twofold: internal surface roughness was reduced (removal of nucleation sites) and the small annulus at each baffle was completely removed (increasing the velocity through the baffle orifice). Overall, we have demonstrated the extended operation of the steady states and produced 884 g (or 141 g/h) of seed crystals of uniform size over 6.25 h.

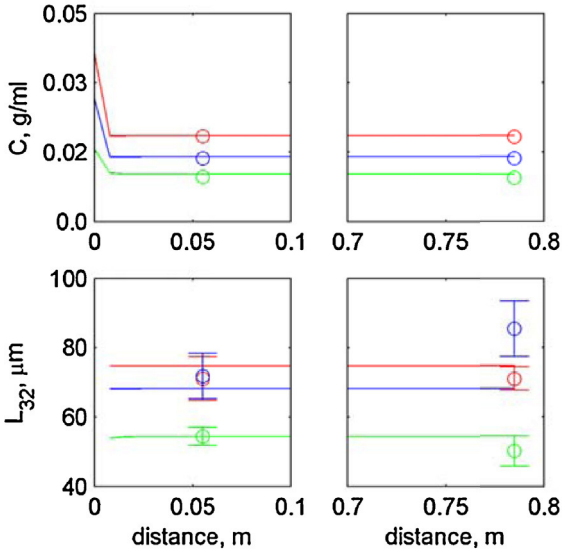

Fig. 5. Comparison of predicted (—) and experimental values (◯) for three antisolvent flow rates, 40 ml/min (red), 60 ml/min (blue) and 80 ml/min (green). Note that the left graphs are associated with the first measuring location, 55 mm away from the mixing point where two streams meet and the right graphs with the second measuring location, 785 mm away from the mixing point. (For interpretation of the references to colour in this figure legend, the reader is referred to the web version of this article.)

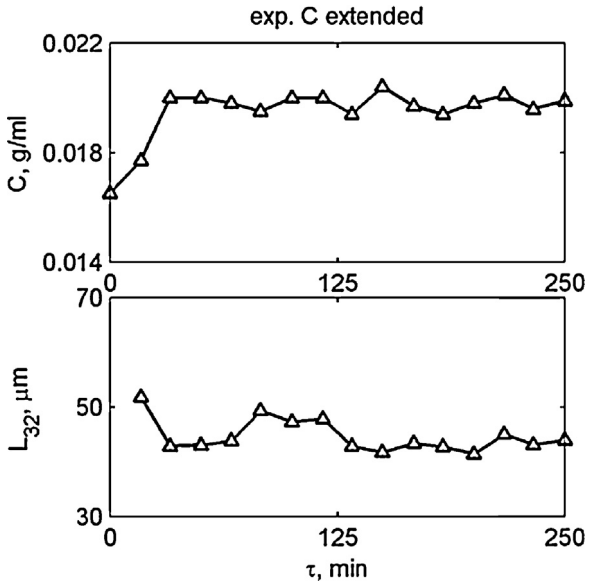

Fig. 6. Measurements of C_2 and $L_{32,2}$ for an extended period of exp. C as a function of τ.

5. Conclusion

From these trials we can conclude the following:

- A minimum oscillatory Re_o is required to ensure suspension of crystalline material and prevention of blockage in this anti-solvent crystallisation at high supersaturations;
- Both temporal and spatial steady states were easily achieved for solute concentrations;
- While the spatial steady states for crystal size were readily achieved, the temporal steady states were much harder to attain, with only one of the trials achieving this for a significant period;
- Rapid desupersaturation of the solution occurred upon mixing with the antisolvent and was observed experimentally and predicted through the population balance modelling;
- The population balance model predicted both the concentration and the mean size, matching experimental data reasonable well;
- Given the right operating conditions, a consistent seed crystal product (in terms of crystal size) of 884 g was produced over 6.25 h of operation.

Acknowledgements

The authors would like to thank EPSRC and the EPSRC Centre for Innovative Manufacturing in Continuous Manufacturing and Crystallisation for funding this work.

References

[1] N. Variankaval, A.S. Cote, M.F. Doherty, From form to function: crystallization of active pharmaceutical ingredients, AIChE J. 54 (7) (2008) 1682–1688.
[2] M. Ståhl, B.L. Åslund, Å.C. Rasmuson, Reaction crystallization kinetics of benzoic acid, AIChE J. 47 (7) (2001) 1544–1560.
[3] J. Gradl, et al., Precipitation of nanoparticles in a T-mixer: coupling the particle population dynamics with hydrodynamics through direct numerical simulation, Chem. Eng. Process.: Process Intensif. 45 (10) (2006) 908–916.
[4] A.F. Blandin, et al., Kinetics identification of salicylic acid precipitation through experiments in a batch stirred vessel and a T-mixer, Chem. Eng. J. (Lausanne) 81 (1–3) (2001) 91–100.
[5] T. Rivera, A.D. Randolph, A Model for the precipitation of pentaerythritol tetranitrate (PETN), Ind. Eng. Chem. Process Des. Dev. 17 (2) (1978) 182–188.
[6] A.J. Alvarez, A.S. Myerson, Continuous plug flow crystallization of pharmaceutical compounds, Cryst. Growth Des. 10 (5) (2010) 2219–2228.
[7] L.L. Simon, A.S. Myerson, Continuous antisolvent plug-flow crystallization of a fast growing API, 18th International Symposium on Industrial Crystallization – ISIC 18, Zurich, Switzerland, 2011.
[8] S. Lawton, et al., Continuous crystallization of pharmaceuticals using a continuous oscillatory baffled crystallizer, Org. Process Res. Dev. 13 (6) (2009) 1357–1363.
[9] Z.K. Nagy, et al., Recent advances in the monitoring: modelling and control of crystallization systems, Chem. Eng. Res. Des. 91 (10) (2013) 1903–1922.
[10] L.L. Simon, et al., Assessment of recent process analytical technology (PAT) trends: a multiauthor review, Org. Process Res. Dev. 19 (1) (2015) 3–62.
[11] N.S. Tavare, Mixing in continuous crystallizers, AIChE J. 32 (5) (1986) 705–732.
[12] J.M. Hacherl, E.L. Paul, H.M. Buettner, Investigation of impinging-jet crystallization with a calcium oxalate model system, AIChE J. 49 (9) (2003) 2352–2362.
[13] A.J. Mahajan, D.J. Kirwan, Rapid precipitation of biochemicals, J. Phys. D: Appl. Phys. 26 (8B) (1993) B176.
[14] Y. Liu, R.O. Fox, CFD predictions for chemical processing in a confined impinging-jets reactor, AIChE J. 52 (2) (2006) 731–744.
[15] X. Ni, et al., Scale-up of single phase axial dispersion coefficients in batch and continuous oscillatory baffled tubes, Can. J. Chem. Eng. 79 (3) (2001) 444–448.
[16] H. Jian, X. Ni, A numerical study on the scale-up behaviour in oscillatory baffled columns, Chem. Eng. Res. Des. 83 (10) (2005) 1163–1170.
[17] X.W. Ni, et al., On the crystal polymorphic forms of L-glutamic acid following temperature programmed crystallization in a batch oscillatory baffled crystallizer, Cryst. Growth Des. 4 (6) (2004) 1129–1135.
[18] R.I. Ristic, Oscillatory mixing for crystallization of high crystal perfection pharmaceuticals, Chem. Eng. Res. Des. 85 (A7) (2007) 937–944.
[19] F.L. Nordström, Å.C. Rasmuson, Solubility and melting properties of salicylic acid, J. Chem. Eng. Data 51 (5) (2006) 1668–1671.
[20] A.D. Randolph, M.A. Larson, Theory of Particulate Processes: Analysis and Techniques of Continuous Crystallization, Academic Press, 1988.
[21] B.J. Ridder, A. Majumder, Z.K. Nagy, Population balance model-based multiobjective optimization of a multisegment multiaddition (MSMA) continuous plug-flow antisolvent crystallizer, Ind. Eng. Chem. Res. 53 (11) (2014) 4387–4397.
[22] M.A.A. Fakhree, et al., Solubility of 2-hydroxybenzoic acid in water, 1-propanol, 2-propanol, and 2-propanone at (298.2 to 338.2) K and their aqueous binary mixtures at 298.2 K, J. Chem. Eng. Data 57 (11) (2012) 3303–3307.
[23] P. Stonestreet, P.M.J. Van der Veeken, The effects of oscillatory flow and bulk flow components on residence time distribution in baffled tube reactors, Chem. Eng. Res. Des. 77 (A8) (1999) 671–684.
[24] C.M. Chew, et al., Crystallization of paracetamol under oscillatory flow mixing conditions, Cryst. Growth Des. 4 (5) (2004) 1045–1052.
[25] X.W. Ni, A.T. Liao, Effects of mixing, seeding, material of baffles and final temperature on solution crystallization of L-glutamic acid in an oscillatory baffled crystallizer, Chem. Eng. J. 156 (1) (2010) 226–233.